Z. Kristallogr. **227** (2012) 63–78 / **DOI** 10.1524/zkri.2012.1438

Multigrain crystallography

Henning O. Sørensen[I, 1, *], Søren Schmidt[I], Jonathan P. Wright[II], Gavin B. M. Vaughan[II], Simone Techert[III], Elspeth F. Garman[IV], Jette Oddershede[I], Jav Davaasambu[III], Karthik S. Paithankar[IV, 2], Carsten Gundlach[II, 3] and Henning F. Poulsen[I, *]

[I] Centre for Fundamental Research: Metal Structures in Four Dimensions, Risø National Laboratory for Sustainable Energy, Technical University of Denmark, Frederiksborgvej 399, P.O. 49, 4000 Roskilde, Denmark
[II] European Synchrotron Radiation Facility, Grenoble, France
[III] Max-Planck-Institute for Biophysical Chemistry, 37077 Göttingen, Germany
[IV] Laboratory of Molecular Biophysics, Department of Biochemistry, University of Oxford, South Parks Road, Oxford, OX1 3QU, UK

Received July 15, 2011; accepted November 2, 2011

Multigrain crystallography / 3DXRD microscopy / Crystal structure determination / Polycrystal diffraction / Crystal indexing

Abstract. We summarize exploratory work on multigrain crystallography. The experimental arrangement comprises a monochromatic beam, a fully illuminated sample with up to several hundred grains in transmission geometry on a rotary table and a 2D detector. Novel algorithms are presented for indexing, integration and filtering with emphasis on handling the complications of spot overlap and the need for on-line analysis. The structure solution and refinement steps are performed by conventional single crystal programs. Simulations are used to verify the algorithms and to probe the overall limitations of the methodology in terms of number of grains, size of unit cell and direct space resolution. First experimental results in the fields of chemistry, structural biology and time-resolved studies in photochemistry are presented. As an outlook, the concept of *TotalCrystallography* is introduced, defined as the simultaneous characterization of the 3D atomic, and 3D grain-scale structure of polycrystalline specimens with phases of unknown composition and structure.

1. Introduction

For a century, crystallographic analysis has been based on either single crystal (Friedrich, Knipping, and Laue, 1912, Bragg, 1912) or powder diffraction (Debye and Scherrer, 1916) measurements. Thus existing methods apply to one of two extremes of sample constitution: a homogeneous, mono-domain specimen, or a mono-dispersed powder comprising a huge number of crystals.

However, many interesting samples are available only in the form of a heterogeneous assembly of a limited number of crystals, perhaps even including several phases of matter. Such samples fall in between the ideals and are inappropriate for crystallographic characterization by normal methods, leading to significant effort in sample preparation. In numerous cases, preparation of suitable single crystals is not possible, *e.g.* in relation to natural objects, studies in extreme environments, studies involving domain formation or reconstructive transitions or more generally cases where suitable crystallization conditions have not been found. In other cases, samples are extremely unstable, making it impossible to collect complete data sets. Modifications of existing single crystal approaches for up to 4 crystals have been suggested (Sparks, 1999; Buts *et al.*, 2004), but these methods cannot be scaled to a larger number of crystals and are far from the "general case" which we aim to address. Furthermore, structures from powder diffraction are typically less accurate than those from single crystals. While substantial improvements have been made in the last decade (Wessels *et al.*, 1999; Harris *et al.*, 2001; David *et al.*, 2002; Baerlocher *et al.*, 2004), *ab initio* structure solution based on powder diffraction data is still highly problematic for structures with more than about 40 atoms in the asymmetric part of the unit cell, and unconstrained refinement of even such moderately complicated structures is not feasible.

To overcome these limitations, in 2004 three of the authors suggested an alternative approach: multigrain crystallography. The experimental arrangement is identical to that typically used in single crystal X-ray crystallography, with a monochromatic beam, a fully illuminated sample in transmission geometry on a rotary table and a 2D detector. First the successful simultaneous structure refinement of 57 grains of α-Al_2O_3 was demonstrated (Schmidt *et al.*, 2003). Next the solution and refinement of the structures

[1] Current address: Nano-Science Center, Department of Chemistry, University of Copenhagen, Universitetsparken 5, 2100 Copenhagen Ø, Denmark.
[2] Current address: Macromolecular Crystallography (BESSY-MX), Institute F-I2, Elektronenspeicherring BESSY II, Helmholtz-Zentrum Berlin für Materialien und Energie, Albert-Einstein-Str. 15, 12489 Berlin, Germany.
[3] Current address: MAX IV Laboratory, Lund University, P.O. Box 118, SE-221 00 Lund, Sweden.
* Corresponding authors (e-mail: osholm@nano.ku.dk, hfpo@risoe.dtu.dk)

of 13 grains out of about 70 illuminated micrometer-sized (average diameter: $\sim$5 μm) grains in a powder of the compound $Cu(C_2O_2H_3)_2 \cdot H_2O$ was reported (Vaughan *et al.*, 2004). In the latter case, the refinement was shown to be on a par with single crystal results and superior to results from state-of-the-art powder diffraction. Diffraction on polycrystalline samples comprised of tens or even hundreds of tiny crystals have been made possible through the development of 3rd generation synchrotrons delivering monochromatic X-rays with a very high brilliance. Furthermore frequently new and improved detectors become available pushing the limits for the crystal size and the number of crystals one can investigate. Even though fascinating improvements in the instrumentation have been made, and are still made, it is also evident from this work that a main limitation for multigrain crystallography will be the overlap of diffraction spots.

Within the project *TotalCryst* (http://www.totalcryst.dk) we have explored the concept of multi-grain crystallography. Here we present an overview of the results, with focus on the following topics:

- Novel approaches for indexing and integration of multigrain data
- A survey of the limitations of the methodology in terms of the number of grains simultaneously illuminated, the size of the unit cell and the direct space resolution.
- As examples of this research, we present applications from chemistry, structural biology and time-resolved photo-chemistry.

As an outlook, we introduce the concept of ***TotalCrystallography.*** The aim is to provide a simultaneous structural characterization of multiphase materials on both the grain scale and the atomic scale. More specifically, it holds the possibility of utilizing three-dimensional X-ray diffraction (3DXRD) microscopy (Poulsen, 2004; Juul Jensen *et al.*, 2006) to generate 3D maps of the grains, visualizing their morphology, orientations and stresses, and at the same time being able to perform a full structural solution and refinement for each grain. Such studies are seen as vital in many areas of material science and geosciences, and may also be relevant for *e.g.* probing the heterogeneity of drug tablets. We will discuss strategies for implementing the vision of *TotalCrystallography* and report some first results.

In this special issue marking 100 years since Laue's discovery that X-rays are diffracted by a crystal, (Friedrich *et al.*, 1913) we present methods to perform crystal structure determination from the individual constituents in polycrystalline samples. An interesting aspect of Laue's work was that, in order to show that the diffraction spots were due to the periodicity of the crystal, Friedrich, Knipping and Laue (1913) crushed the crystal and illuminated the crushed sample, finding that the distinct spots were no longer present. They did notice that weak spots were present on their photograph and concluded that these small remaining freckles were due to fragments of the original crystal. Thus, multigrain crystallography has been possible since the discovery of X-ray diffraction, but it is only now, 100 years later, that we are able to analyze and determine structures from such data. Friedrich, Knipping and Laue (1913) furthermore demonstrated that the spots on the detector were projections of the illuminated part of the crystals. This is the very property which is used in 3DXRD microscopy for determining the morphology of the crystals buried in a polycrystalline sample (Poulsen *et al.*, 2011).

2. Overview of approaches for multigrain crystallography

The main challenge of multigrain crystallography is the mathematical and computational complexity of the data analysis. The analysis procedure is naturally divided into two parts: 1) indexing, harvesting and filtering data and 2) structure solution and refinement. Generally speaking, several iterations of the two parts are performed.

The first part is dealt with by FABLE (Fully Automatic BeamLine Experiments), which is a suite of programs developed by the authors and is the main topic of this paper. FABLE is an open-source software package complete with a graphical user interface, options for use of parallel computing and GPUs, documentation, and a developers corner (http://fable.wiki.sourceforge.net/). A presentation of the computational aspects of FABLE as well as some of the mathematical aspects of the individual programs will be given elsewhere (Hansen *et al.*, 2009; Schmidt, 2010). The output from FABLE is a list of indexed grains, each with an associated list of reflections and integrated intensities.

The second part, structural solution and refinement, is performed by state-of-the-art single crystal crystallography programs, by either treating each grain as a separate single crystal or by basing the refinement on the complete data set (in which case the scale factors have to be included in the fit). Evidently the first approach can be used also in cases where grain structures vary. In the examples presented below we used *MOSFLM* (Leslie, 2006), *Jana* (Dusek *et al.*, 2001; Petricek and Dusek, 2004) and *SHELX97* (Sheldrick, 2008).

Experience has shown that overlap of diffraction spots originating from different grains is a major limitation of the technique. For this reason we distinguish between two approaches to multigrain crystallography:

- *Low fraction of spot overlap* (as a rule of thumb: up to 15%). In this case one can rely on overlapping spots being filtered out based on their erroneous center-of-mass or integrated intensity. Our work on this approach is presented in Sections 3 and 4.
- *Medium fraction of spot overlap* (up to 50%). In this case overlapping spots are either separated by segmentation, or the shared integrated intensity is used as a constraint in a simultaneous refinement of all contributing grains. Our work on this approach is presented in Section 5.

All algorithms apply to all space groups. For simplicity, in Sections 3–5 below, we shall assume that the sample is mono-phase and the detector is a true far field detector with negligible shifts of diffraction spots due to the position of the grain.

3. Peak searching and indexing

3.1 Data reduction

The 2D image data recorded on the area detector can be efficiently compressed into a list of peaks for cases of low spot overlap and at the same time transformed into a standard FABLE co-ordinate system. For this procedure FABLE includes a full suite of GUIs for preprocessing, peak searching (Wright, 2005), calibration, and indexing (Schmidt, 2010; Wright, 2005). The calibration procedure is interactive and results in a fit of the incident wavelength, the detector tilts and distance, the pixel size, the center of the diffracted signal and a potential mis-alignment of the rotation axis. Peak searching is performed in two steps: first diffraction spots are identified as connected components in (y_{det}, z_{det}, ω) space, where (y_{det}, z_{det}) are detector coordinates and ω symbolizes the rotation. This is performed by a threshold operation which is extremely fast and therefore suitable for online analysis. Next, the center-of-mass coordinates are transformed into diffraction vectors (*G*-vectors) associated with reciprocal space coordinates.

With respect to peak searching with larger amounts of spot overlap, scenarios can easily be imagined in which there are no simple operations sufficient to segment the diffraction spots. In the next stage of sophistication, the information from several thresholds can be combined in a sort of watershed algorithm. Such an algorithm has been implemented by R. Huizenga and coworkers at TU Delft, The Netherlands. This algorithm is particularly superior when it comes to separating relatively sharp (round and small) diffraction spots, such as undeformed samples with many grains in the diffracting volume. Currently the most sophisticated and most time consuming algorithm, DIGIgrain, is a 3D connectivity peak search employing several thresholds which has been developed by Kenesei *et al.* (2010). This routine is especially useful in materials science for segmenting broad diffraction spots from deformed materials with large orientational gradients within the individual grains.

3.2 Indexing with known space groups: Orientation finding

The unit cell of the material may be known *a priori*, *e.g.* as the result of a traditional powder diffraction analysis applied to the polycrystalline data (Schmidt *et al.*, 2003; Vaughan *et al.*, 2004). Indexing in this case means finding the orientation matrices of the grains in the sample and sorting the *G*-vectors according to the grain of origin. Following the presentation of the program *GRAINDEX* (Lauridsen, 2001) in 2001, several alternative approaches have been proposed (Schmidt, 2010; Wright, 2005; Ludwig, 2009, Moscicki, 2009, Lyckegaard, 2010). Some of these rely on the use of direct space information on grain position, derived either from a near field detector (Ludwig, 2009, Moscicki, 2009) or from scanning of the sample (Lyckegaard, 2010). While such methods are relevant for 3D materials science studies, they are of less interest for crystallographic studies, where the size of the entire polycrystalline sample may be a few μm or less. Hence, we shall restrict ourselves to indexing based on orientation and intensity relationships between *G*-vectors. FABLE contains GUIs for two such indexing programs: *ImageD11 indexing* (Wright, 2005) and *GrainSpotter* (Schmidt, 2010).

The indexing approach in *ImageD11* is straightforward: angles between pairs of *G*-vectors are compared to a list of theoretical angles for the known crystal symmetry. Groups of *G*-vectors with mutually consistent angles define grains. This approach is permutative in nature and as such works well when the number of *G*-vectors is relatively small. Peaks are assigned to grains according to an error criterion which measures how close their (h, k, l) indices are to being integers. Grains are then accepted, or not, depending on the total number of peaks for which they can account. Simulations have shown that this algorithm can provide valid results for at least 250 simultaneously illuminated grains of cubic symmetry, equal size and random texture.

The core of *GrainSpotter* (Schmidt, 2010) is an engine for indexing *G*-vectors. The number of computations in this engine scales theoretically linearly with the number of measured *G*-vectors. Uniquely, the program uses a combination of two representations of orientation space: Rodrigues space (Frank, 1988) for local operations and quaternion space (Meister and Schaeben, 2005) for global operations. Grains are indexed by segmenting orientation space (either systematically or randomly) into sub-volumes, local Rodrigues orientation spaces, and for each sub-volume (its size is user defined) identify possible grain orientations without searching the full 3D volume. Furthermore, each candidate *G*-vector, for the sub-volume in question, is used only once. Grains are defined mainly by a completeness criterion on the ratio between observed and expected *G*-vectors. In connection with the use of look-up tables and code optimizations, this has enabled the processing speed to be increased by more than two orders of magnitude as compared to *GRAINDEX*. Centre-of-mass positions of the grains are fitted simultaneously with the grain orientation in the indexing procedure. Another unique feature of *GrainSpotter* is a pseudo-twin filter. These pseudo-twins arise when the crystallographic symmetry is high; in this case a sub-set of *G*-vectors associated with a given orientation can form a pattern consistent with another orientation which is not crystallographically equivalent at a completeness of up to 40%. By adding reflections from other grains, which are arbitrarily positioned in the vicinity of the theoretical *G*-vectors, false grains with a completeness above 50% may appear if this filter is not applied.

In favorable conditions *GrainSpotter* has been demonstrated to be able to handle up to 1000 grains at a time. Various applications of *GrainSpotter* are presented below: for other applications in *e.g.* materials science and geosciences see references (West *et al.*, 2009; Oddershede *et al.*, 2010; Poulsen *et al.*, 2011; Oddershede *et al.*, 2011) and (Sørensen *et al.*, 2011), respectively.

3.3 Generalization to the case of an unknown space group

It is the ambition of the authors that the FABLE software will eventually not need to rely on the *a priori* determination of the unit cell. Notably, only the algorithms for

indexing need modification to achieve this objective. So far two approaches have been explored:

3.3.1 Indexing based on an FFT approach

For large unit cells, the low order diffraction rings might be hidden completely behind a beamstop, or the powder rings may be very close together. However, there will be very many lattice repeats within a collection of diffraction spots. In order to more easily identify the primitive lattice vectors in these cases a Patterson function can be computed using an FFT algorithm, as is commonly already used for indexing in protein crystallography (Campbell, 1998; Powell, 1999). In comparison to reciprocal space based indexing schemes, these real space approaches have the advantage that diffraction spots can be divided into groups using only a partial solution containing a single lattice vector. Using the formalism of Busing and Levy (1967) this can be seen from the indexing equation, $H = (\boldsymbol{UB})^{-1} \cdot G$. Peaks in the Patterson function correspond to lattice vectors in real space and rows of the $(\boldsymbol{UB})^{-1}$ matrix. The observed G-vector data can therefore be tested against a single vector to see whether they generate an H vector with integer indices (h, k, l) where the h index is independent of k and l, and are grouped accordingly. For small numbers of grains, the vectors can even be chosen in a combinatorial algorithm for generating trial orientation matrices. The combinatorial method has been implemented in the *index_unknown.py* script in *ImageD11* (Wright, 2005). Grains are accepted according to a user defined fraction of the total number of peaks that are indexed at a particular *hkl* error tolerance. Each time a new grain is accepted, the indexed peaks are removed from the dataset and the procedure is repeated to find further grains. The removal helps in the relatively common case of larger dominant grains. Currently the program works with extracted peak positions, but it could be adapted in the future to carry out a transform of the diffraction images.

Figure 1a shows the peak positions in reciprocal space for a small wedge of data simulated for a collection of five crystals, all having different unit cell parameters and orthorhombic or monoclinic symmetry. In practice, indexing problems are usually easier than this test example as a solution can be confirmed when the same unit cell is recognized in several orientations. Furthermore, it is usual to start by indexing the strongest peaks found at high angles that originate from the largest grains in the sample. Once a unit cell has been identified, the methods from the previous section can be used to find the rest of the orientations corresponding to the more abundant weaker peaks.

3.3.2 Indexing based on pattern recognition

The indexing program *GrainSpotter* (Schmidt, 2010) has an option for indexing diffraction data with unknown unit cell and lattice structure. Ideally, the diffraction data arising from N crystallites is the superposition of the diffraction from N rotated but otherwise identical base lattices.

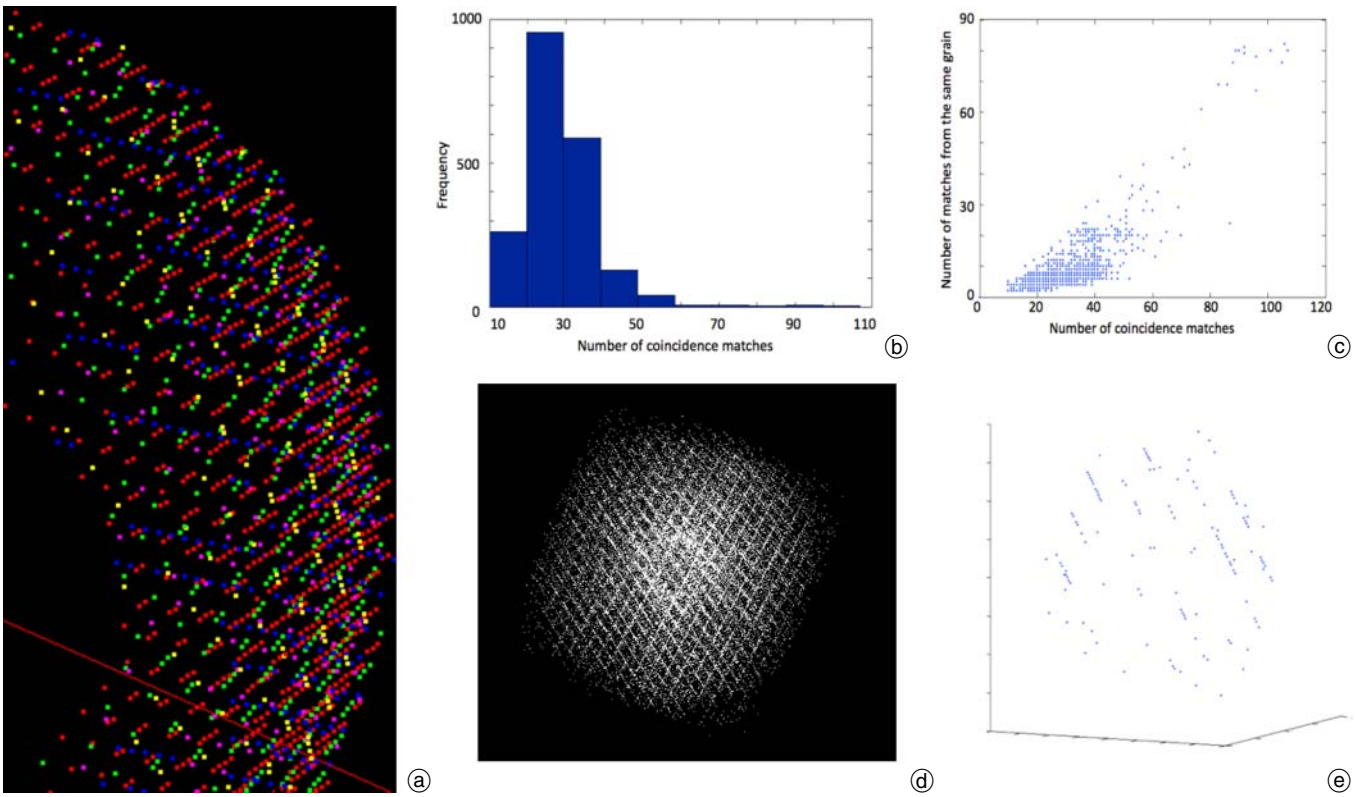

Fig. 1. Indexing in the case of unknown unit cells. (**a**) Simulation of five different intersecting lattices from a 5° wedge of diffraction data. The FFT based algorithm in *index_unknown.py* has identified the five orientation matrices which were used to color code the spots. (**b**)–(**c**) Simulated data set of aluminum with 100 crystallites and 2000 randomly chosen rotations with *GrainSpotter*. (**b**) Distribution of matched measurements per rotation is shown. (**c**) The number of matched measurements from the same crystallite, identified using the Monte Carlo truth in the simulated data, is given. (**d**) The lattice points extracted from an experimental data set of 12 crystals of the "unknown" compound 2-benzyl-5-benzylidencyclopentanone (BBCP). (**e**) An example of a base lattice from the indexing procedure.

By rotating the full data set and matching the rotated data points with respect to the un-rotated data points, occasional matches between different replicas of the base lattice will occur, revealing the orientation difference between two crystallites.

In practice, the same indexing engine in *GrainSpotter* is used for indexing both known and unknown unit cells. In the latter case the set of theoretical scattering vectors is replaced by the data set itself. Figures 1b and c show an example of the results of the pattern recognition method using simulated data of a simple structure, aluminum, with 100 grains. The distribution of coincidence matches from 2000 randomly chosen rotations (Fig. 1b) and has a peak at around 30 coincidences, which can be seen as noise. A second peak is found with close to 90 matches: these are candidate grains to be used in the subsequent data analysis. By comparing the known solution with the simulations, it can be seen (Fig. 1c) that a low number of coincidences indicate a high likelihood of a false lattice and that a high number of coincidences indicates a high likelihood of a correct match of base lattices. These results are encouraging.

In Figs. 1d and e we show the results of an analysis of real data collected on 12 crystals of the compound 2-benzyl-5-benzylidene-cyclopentanone (BBCP). Details of the data collection are given in Section 7.3. 10000 randomly chosen orientations were tested using only the inner part of reciprocal space. The candidate grain with the highest number of coincidences (133) turned out to provide excellent figures-of-merit. Using Dirax (Duisenberg, 1992) the unit cell parameters were determined to be: $a = 8.643$ Å, $b = 10.630$ Å, $c = 31.378$ Å, $\alpha = 90.01^\circ$, $\beta = 90.24^\circ$, $\gamma = 90.14^\circ$, in good agreement with the unit cell parameters ($a = 8.634(1)$ Å, $b = 10.642(2)$ Å, $c = 31.224(6)$ Å) determined in a previous single crystal experiment (Davaasambuu *et al.,* 2005).

The pattern recognition method offers additional noise filtering by matching several high coincidence solutions into a base solution (by rotating solutions into a common frame). The high frequency lattice points in the base solution, *i.e.* points present in many lattices, are then kept for use in determining the unit cell. It is foreseen that the method will be able to handle samples consisting of multiple phases, although this possibility has not yet been tested.

4. Integration and filtering

The procedure described in Section 3.1 is incomplete for two reasons. Firstly, the integrated intensities were found by simply summing the pixel intensities in the pixels above the threshold. Peak integration based on profile fitting typically leads to better results for the weaker peaks than simple summation, as the shape of weak and thereby noisy peaks is difficult to estimate (Graafsma *et al.*, 1997). However very good results can sometimes be obtained (Sørensen and Larsen, 2003) by simple summation if the crystal morphology is used to define the peak shape, as can be done in a program such as EvalCCD (Duisenberg, 1998). Secondly, as discussed in detail below, a main limitation of multigrain crystallography is spot overlap. In that context, the heterogeneity in size and the perfection of the grains play an important role. Hence, it is to be expected that the illuminated grains diffract to different *d*-spacings. This leads to two "noise-terms":

- Spots identified by *peaksearch* which cannot be identified by the indexing program.
- Spots which are below the intensity threshold employed by *peaksearch*. These essentially act as a strongly varying background, which tend to corrupt the integrated intensities.

To address these issues, FABLE includes a set of integration and filtering modules, which can be used iteratively with the indexing modules:

- A peak integration module: *Fabric* (Sørensen, 2007). This module operates in three modes: 1) a conventional "shoe-box" approach where the summed intensity is found within a box, the size of which is specified by the user, 2) a statistical approach whereby the peak and background pixels inside the "shoe-box" are determined using a Baysian analysis (Straasø *et al.*, 2011), and 3) a novel approach for integration based on peak shapes. The latter is described in detail in Section 5.1.
- A filtering and fitting module *FitAllB* (Oddershede, 2010). The algorithm is a robust 12-parameter-per-grain fit of the centre-of-mass grain positions, orientations and stress tensors including error estimation and outlier rejection. This module is also of interest for the materials science community, since it provides a way to determine the stress in individual grains. In a demonstration experiment 2000 grains were characterized with a resulting resolution of approximately 3 μm in position, 0.05° in orientation and 10^{-4} in strain, respectively (Oddershede, 2010).
- A module for assigning peaks to grains and making centre-of-mass grain maps *makemap.py* (Wright, 2005). Diffraction peaks are assigned to the grain which gives the most accurate predicted position in reciprocal space and then the positions and orientations of the grains are refined.

Extracted intensities may subsequently be sorted, filtered and merged based on the crystal point group. If the sample is crystallographically homogeneous, the different crystals may also be scaled and merged together in order to create a single data set. The procedure has been described in Vaughan *et al.* (2004) and implemented in a series of programs (Vaughan, 2008).

The peaks are first sorted by point group, with peaks having too few or too many pixels, those near the rotation axis, those having peak intensities exceeding the dynamic range of the detector and those not allowed by space group being eliminated. Intensities are corrected for Lorentz and polarization factors. Additionally it is possible to correct for lost intensity below the threshold by estimation of a peak shape function from the measured data, either based on the extrapolation of an analytical fit, or via a learned empirical function, as described in Section 5 in the case of overlapping peaks.

If the data for each crystal in the sample are sufficiently redundant, it is possible to perform robust intra-crystal filtering based on equivalent statistics. The data can then be

scaled by comparing the relative intensities of equivalent families, and a single data set can be produced by merging the data from all of the crystals, if appropriate. At each step outlier elimination must be carried out. As the outlier distributions are generally highly asymmetric, care must be taken regarding the central tendency indicator chosen for outlier elimination, with either the weighted mean, median or most-likely-value (the mode of the histogrammed distribution) being the most appropriate depending on the data set.

The origin of the asymmetry in the distribution is twofold. Particularly in samples with many crystals, peaks from other crystals will be coincidentally found at lattice points in reciprocal space. Those coming from unindexed crystals create a tail on the high side of the distribution. The tail on the low side of the distribution is due to imperfect treatment of the background. Currently backgrounds are estimated by using either the pixel-by-pixel through the image series median or minimum value. Neither is totally satisfactory, the first tending to overestimate, and the second to underestimate, the true value. In either case, the weakest peaks are the most affected.

By filtering and down weighting outliers, it is possible to obtain symmetric distributions of equivalent intensities. The width of these intensity distributions can then be used to more accurately determine the gain of the system, thereby making it possible to convert the measured intensities into counts, and produce proper weights.

Having carried out these steps, it is generally advantageous to use the set of filtered, weighted peaks to redetermine orientation matrices and global parameters, and to loop through the procedure a second time in order to produce a final data set. This has been carried out on several different kinds of data sets, as described in 7.1 and in more detail in Vaughan (2011).

5. Algorithms for medium fraction of overlapping spots

For larger fractions of spot overlap we suggest to determine accurate peak profiles for every spot based on the well characterized peaks. In this way the degree of spot overlap can be determined. The intensity of the overlapping spots may then be separated into parts arising from contributing grains, and solution and refinement may proceed independently for each grain. Alternatively, the shared integrated intensity may be used as a constraint in a simultaneous refinement of all contributing grains.

5.1 Generation of peak profiles based on single grain ODFs

We shall assume that the instrumental resolution function is known, and that the peak profile in the radial direction is completely determined by the radial component of this resolution function. In the two other directions in reciprocal space, the peak profile is a convolution of contributions from the instrument and the sample. The latter 2D intensity distribution we shall term the "mosaic spread".

The key in this approach is to realize that the mosaic spread by definition is a projection of a distribution in 3D orientation space: the single grain orientation distribution function (ODF) for the grain in question. For each grain, the single grain ODF can be reconstructed from a set of mosaic spreads associated with a set of reference reflections. These reflections are chosen to avoid overlap: typically they have high *d*-spacings and low multiplicity. Conventional algorithms for the generation of ODFs as used by the texture community (Kochs *et al.*, 1998) do not apply to a single grain ODF. Instead, a novel ODF iterative conjugate gradient reconstruction method using a pre-conditioner was introduced. The details of this algorithm are presented in Hansen *et al.* (2009), where it is also demonstrated that 15 reference reflections may be sufficient to generate a high quality ODF.

Once the single grain ODFs are known, we can determine the mosaic spread (and thereby the peak profile) of any reflection by an integration of the relevant ODF in a direction given by the grain orientation and the position of the reflection in reciprocal space (Hansen *et al.*, 2009). This makes it easy to determine which diffraction spots are overlapping. For overlapping spots, the pixel intensities can be distributed between the contributing reflections based on a combined fit.

To illustrate the approach and provide first results, we chose to work on an undetermined crystal structure, 4-(6-chloro-3-phenyl-indan-1-yl)-1,2,2-trimethyl-piperazine succinate, using a lumpy sample of 25 μm size. From the X-ray data it was evident that the sample comprised two crystals, which diffracted to 0.84 Å, as well as a number of inferior crystals. The two crystals could be indexed using *index_unknown.py* from *ImageD11* (Wright, 2005), leading to a monoclinic unit cell with the parameters: $a = 6.050$ Å, $b = 9.076$ Å, $c = 44.336$ Å, $\alpha = 90.00°$ $\beta = 82.16°$, $\gamma = 90.00°$. This unit cell could be transformed to an orthorhombic unit cell with the parameters: $a = 9.076$ Å, $b = 6.050$ Å, $c = 43.922$ Å, $\alpha = \beta = \gamma = 90.00°$. The most probable unit cell is the monoclinic cell as the $0k0$, $k = 2n + 1$ seems to be systematically absent. The mosaic spreads of the two indexed crystals were of the order of 2°.

Figure 2 illustrates the analysis procedure for one of the grains. Figure 2A shows an area-of-interest on the detector around a specific reflection as a function of the rotation angle. From these data a 2D map of the mosaic spread can be constructed (integrating over the radial direction in the images); this is called a *u,v*-map. 16 strong reflections associated with this grain with no apparent overlap were identified. Based on the *u,v* maps of these standard reflections, the single grain ODF was reconstructed using the module *fabric* (Sørensen, 2007). For all reflections related to the grain, the corresponding peak profile as a projection of the ODF can be estimated. As an example of the quality of such profiles, the projection of the standard reflection is shown in Fig. 2B and C. For all 16 standard reflections the projected peak shapes were accurate to a high precision. Having verified the quality of the peak profile prediction in this way, the ODF was then used to simulate peak profiles for all reflections.

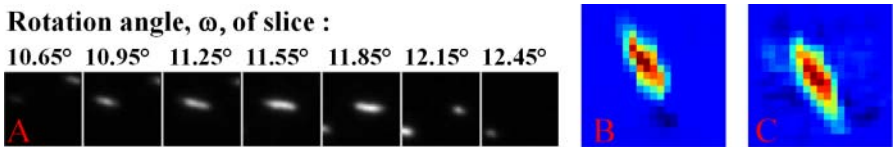

Fig. 2. Determination of the peak profile for reflection (−2, 2, 11) for one of the grains in the sample of 4-(6-Chloro-3-phenyl-indan-1-yl)-1,2,2-trimethyl-piperazine succinate. (**A**) raw data of the diffraction spot as function of rotation angle. (**B**) *u,v*-map generated based on the raw data. (**C**) projection of the resulting single grain ODF: a simulation of the peak profile for the reflection in question.

Using this procedure we integrated 6074 reflections of which 1723 were unique. The residuals were found to be fairly high: R_{int} was 0.158 and R_σ was 0.106. Attempts to solve the structure based on these data with *SHELXS97* (Sheldrick, 2008) were unsuccessful. We speculate that the high mosaicity indicating that the crystal is in fact highly disordered could be the reason. But the reason could also be due to an incorrect determination of the space group.

5.2 Constrained refinement

The constraint that a given integrated intensity is the sum of contributions from several grains can be used in a simultaneous refinement of the contributing grains. Evidently, with such constraints the refinements of all grains may be coupled. The refinement program JANA (Dusek *et al.*, 2001; Petricek and Dusek, 2004) was modified to expedite this task, using the output of *fabric*.

Simulations on *R*(+)-2-phenoxypropionic acid (a monoclinic system with a unit cell volume of 417 Å^3) (Sørensen and Larsen, 2003) provided encouraging results. As an example we considered a sample of 40 grains with a log-normal grain size distribution in which 53% of the simulated peaks were overlapping. In this case crystal refinement with JANA produced scale factors for all grains which were within 1% of the true values. The residual of the refinement was less than 2%.

Our preliminary conclusion based on the results described in 5.1 and 5.2 is that the technique of constrained refinement seems easy to apply and well adapted to the problem of spot overlap. With respect to peak fitting, this approach needs further work. The single grain ODF formalism is stringent, but with the angular resolution provided by standard diffractometers, it tends to require such large mosaic spreads that the crystals have an inherent low quality. One solution may be to take an independent set of data with the detector positioned further away from the sample. Other solutions may be to generalize existing methods for integration based on peak profiles (Kabsch, 1988; Leslie, 1992; Otwinowski and Minor, 1997; Schreurs *et al.*, 2010).

6. Simulations to determine the limitations of the technique

It is evident that the fraction of overlapping diffraction spots will increase with the number of grains simultaneously illuminated, the size of the unit cell and the direct space resolution. FABLE includes a powerful simulator (Sørensen, 2008; http://sourceforge.net/apps/trac/fable/wiki/PolyXSim), which has been used to estimate the range of applicability of multigrain crystallography with respect to these parameters.

The simulations were all performed at an incident wavelength of 0.9395 Å. The specimens were assumed to be fully illuminated and to be so small that the shifts of diffraction spots due to the position of the grains within the sample are negligible. For this test all grains were assumed to have the same size and random orientations. Based on a conservative estimate, we specified that reflections could potentially overlap if they are displaced by less than 0.4° in ω and within 11 pixels either vertically or horizontally on the detector. Using specifications from an ADSC Quantum Q315r detector, the detector used in the simulations below is assumed to have 3072 × 3072 pixels with a pixel size of 102.6 μm. The sample-to-detector distance was set to either 5.15 cm, 23.2 cm, or 37.9 cm, corresponding to a resolution of $d_{\text{min}} = 0.8$ Å, 1.6 Å and 2.4 Å, respectively, at the edge of the detector.

Four samples were simulated:

1. Aluminum (space group $Fm\bar{3}m$, cubic $a = 4.0497$ Å, unit cell volume: 66.4 Å^3)
2. BBCP: 2-benzyl-5-benzylidencyclopentanone (space group *Pbca*, orthorhombic $a = 10.790$ Å, $b = 8.70$ Å, $c = 31.34$ Å, unit cell volume: 2942 Å^3)
3. Crambin (space group $P2_1$, monoclinic $a = 40.82$ Å, $b = 18.49$ Å, $c = 22.37$ Å, $\beta = 90.47°$, unit cell volume: 16880 Å^3)
4. Lysozyme (space group $P4_32_12$, tetragonal $a = 78.5$ Å, $c = 36.9$ Å, unit cell volume: 227400 Å^3)

The results for the fraction of overlapping reflections are shown in Fig. 3. Not surprisingly, the curves representing overlap fraction are initially approximately linear with the number of grains illuminated, while for large numbers of grains they asymptotically approach 100% overlap.

By calibration to experimental data, cf. Section 5, as a rule-of-thumb we state that the simple "algorithms for low fraction of spot overlap" presented in Section 3 will work well for overlap fractions below 15%, while the encouraging results for constrained refinement presented above suggest that 50% overlap may be acceptable for this approach. It appears that (for a 2K CCD detector) 1000 grains are within reach for simple metals, and a few hundred grains for typical small organic molecules, while of order 10 protein crystals can be handled simultaneously. Notably, these limits will be the same in case of polymorphs (although the indexing will of course be more complex). For multiphase materials and lower symmetry space groups the overlap fraction actually decreases, since the diffraction spots will be more evenly spread on the detector.

Two limitations should be highlighted. In the case of severe texture the overlapping fraction will increase. Like-

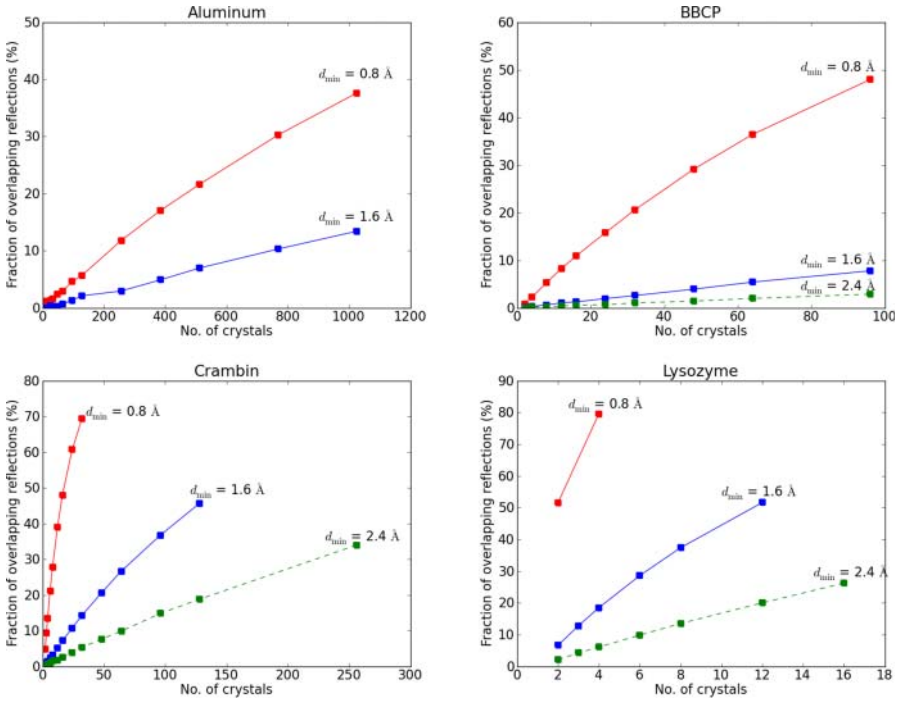

Fig. 3. The simulated fractions of overlapping reflections are shown as a function of data resolution, $d_{\min}$, and number of crystals for the four chosen structures.

wise, the typical log-normal grain size distribution implies that grains will diffract to very different direct space resolutions and some grains may simply be too small to be observed at all. However, this is mainly a concern in materials science and geosciences, while structural solution and refinement for the larger crystals would generally only be satisfactory for applications in chemistry and structural biology.

On the other hand, the specifications used in the simulations may be seen as conservative, in particular if the overlap is dominated by the instrumental resolution rather than grain specific issues such as mosaicity and size broadening. Often spots can be as close as 6–7 pixels and still be clearly separated. This may improve the overlap fraction by a factor 2–3. Likewise, the overlap fraction can be made 2–4 times smaller by placing the detector at twice the distance away. Evidently fewer of the diffraction spots will be observed in this case, but provided the grains belong to the same phase, there will be ample redundancy. Developments in detector technology, particularly pixel detectors, will allow more spots to be recorded in a single frame without overlap, so that problems with larger unit cells and more crystals may be addressed in the future.

In this context it is also illustrative to consider experimental results on cubic insulin (Paithankar *et al.*, 2011). Four crystals were picked up in a single cryoloop and irradiated simultaneously. The simulations shown in Fig. 3 on tetragonal lysozyme, which has the same density of reciprocal lattice points as cubic insulin, show that a fraction of 12–15% of the recorded reflections are expected to be overlapped. Paithankar *et al.* (2011) actually performed simulations on the cubic insulin and reached the same conclusion. On the other hand, for the experimental data the problem with overlapping reflections seems almost insignificant in the integrated data. A high degree of overlap would be expected to result in a high number of rejected reflections based on irregular spot profiles, but far less than one percent (1603 reflections out of 270633 collected reflections) were rejected. It could be argued that the overlapping reflections are not identified by comparison of the spot profiles, but even if that is the case the influence on the final data set is minimal. since very respectable residuals are obtained, *e.g.* $R_{\rm meas}$ is about 10% for each of the four data sets. Furthermore, no peculiarities were found in the crystal structures refined against these data. This suggests that our simulations are very conservative in estimating the problem of overlapping reflections and indeed even larger problems, more crystals and larger unit cells, might be within reach. It also suggests that the errors introduced are fundamentally statistical, *i.e.*, they lower the quality of residuals and the precision of refined parameters, rather than systematic.

7. Applications of multigrain crystallography

Within the *TotalCryst* project, emphasis was on applications for three specific disciplines. Our findings are summarized below:

7.1 Small molecule applications

Structure determination by X-ray diffraction methods is one of the best ways of establishing the molecular structure and the stereochemistry of natural and synthetic compounds. Crystallization of chemical compounds is one of the bottlenecks in structure determination. Hence, if we could determine the structure from a conglomerate of crystals without testing the quality of the crystals individually, it would facilitate the speed of structure determination tremendously. If large single crystals are not formed, the typical remedy is to change the crystallization conditions, but this may lead to a different polymorph of the compound (for a recent overview see *e.g.* Bernstein (2002)). In

the pharmaceutical industry it is important to determine the structure of the compound crystallized under the same conditions as used for the product, to ensure that it is the structure of the same polymorph which is determined. Currently we have shown that we can use multicrystal crystallography to determine the structure of a few small molecules, including a simple metalorganic compound, cupric acetate monohydrate (Vaughan *et al.*, 2004), and two organic molecules, BBCP (see Section 7.3) and tetrathiafulvalene-*p*-chloranil (TTF-CA).

One of the most important motivations for developing a multigrain method to determine structures from polycrystalline samples was to obtain structures of a quality comparable to structures determined by single-crystal X-ray diffraction methods. In the study of cupric acetate monohydrate Vaughan *et al.* (2004) performed a careful analysis and comparison of the structural results obtained by traditional high resolution powder diffraction with the new multigrain crystallography approach. The quality of the two structures was compared to the high quality structure determined from a single crystal. Here we will briefly summarize the results of that study. The multicrystal sample was prepared by placing about 70 crystals on a glass needle in grease. At this stage the indexing routines were only able to process data with a known unit cell. Therefore the diffraction data were transformed into a pseudo-powder pattern from which the unit cell and space group of the structure were determined. Using these parameters GRAINDEX indexed the diffraction pattern and 13 crystals were indexed with full completeness, *i.e.* all expected *G*-vectors of the lattice were found in the set of *G*-vectors obtained from the experiment. The reflections were sorted, filtered and merged into one data set. These data had, compared to usual single-crystal data, a fairly high R_{sym} of 0.136, but it was anyway possible to solve and refine the crystal structure to a good accuracy. The final model, refined with *SHELXL* (Sheldrick, 2008) to give R_1 of 0.057 ($wR_2 = 0.128$), included positions and anisotropic mean-square displacement parameters (ADPs) of all non-H atoms and the H atom positions of the water molecule (initial positions determined from the difference Fourier map). The methyl group hydrogen atoms were refined with a riding model. This differs somewhat from the model refined against the powder diffraction data. In that case the refinement led to non-physical parameters for the ADPs for carbon atoms, hence they were modeled with isotropic mean-square displacement parameters. Similarly, it was not possible to refine the H atom positions freely, though their approximate positions could be located in the difference Fourier map. Comparison of the multigrain structure and powder diffraction structure to the single-crystal structure, showed that the root-mean-square deviation of all positions were 0.0178 Å and 0.0350 Å, respectively. The comparison of the thermal parameters shows that the parameters obtained from multigrain compares about 10 times better than the ones obtained from the powder experiment. Furthermore, the deviations in bond distances is 2–3 times smaller for the multigrain structure compared to the powder structure.

Recently, improvements in the merging procedure have been made as described in Section 4. With these, better fits have been obtained for several small molecules and inorganic systems. For example 26000 peaks from 31 crystals of Na $(H_2PO_4) \cdot 2\,H_2O$ could be merged with an R_{sym} of 2.6%, and up to 1 million peaks from samples with several hundred crystals were merged into high quality data sets. Details can be found in Vaughan (2011).

7.2 Structural biology

Macromolecular crystallography (MX) has undergone huge developments during the last 20 years, improving options for single crystal diffraction through progress in crystal growth methods, systematic procedures for cryo-cooling and better instrumentation, *e.g.* radiation sources. The multicrystal methods presented in this paper enable new ways of enhancing the data collection procedures and improving the data quality to obtain structures of bio-molecules.

One of the main challenges in MX is radiation damage, which is unavoidable when employing synchrotron radiation even with the sample held at 100 K (Ravelli and Garman, 2006). Within the *TotalCryst* project we have explored the option of collecting data on several crystals simultaneously during a limited sample rotation. As the crystals have different orientations, it is feasible in this way to extract a merged low-dose data set comprising reflections filling most of orientation space (Paithankar *et al.*, 2011).

In an experimental feasibility study on 4 crystals of cubic insulin mounted in a single cryoloop (Fig. 4a), data were collected over 90° of rotation. As a result of the multigrain analysis, the data set for each of the crystals had an R_{meas} between 0.08 and 0.14 and $R_{p.i.m.}$ of about 0.03 to a resolution of 1.9 Å. By merging the data sets from the four crystals into one, we found that a reduced data set with the same quality descriptors could be obtained by using data from the only the first 12° of rotation (Fig. 4b). Based on wedges representing every 15° of rotation the data were merged and a structural model was refined leading to an *R*-value of 0.153(1) for the data from each of the six rotation subsets. No radiation damage was observed. If the protein structure degrades during the data collection, it would be possible to follow the structural evolution as a function of dose. This work is similar in concept to the previous study of Berglund *et al.* (2002) where data were collected from 9 different single crystals starting in orientations differing by 10° each, so that composite datasets consisting of 9 wedges 10° at the same dose could be assembled, but the multicrystal approach removes the need for more than one data collection.

Another possible benefit from our approach is that the diffraction quality of several crystals can be tested at once. As a demonstration, seven chicken egg-white lysozyme crystals were mounted in a cryoloop, and the sample was centered to illuminate most of the crystals. All seven crystals could be indexed by *GrainSpotter* using the low order reflections, but only datasets for four crystals could be integrated to a resolution of about 2 Å. Three of these data sets were of low quality due to imperfect crystals: they had high mosaicity and the diffraction spots clearly became more and more diffuse as the sample was rotated. The

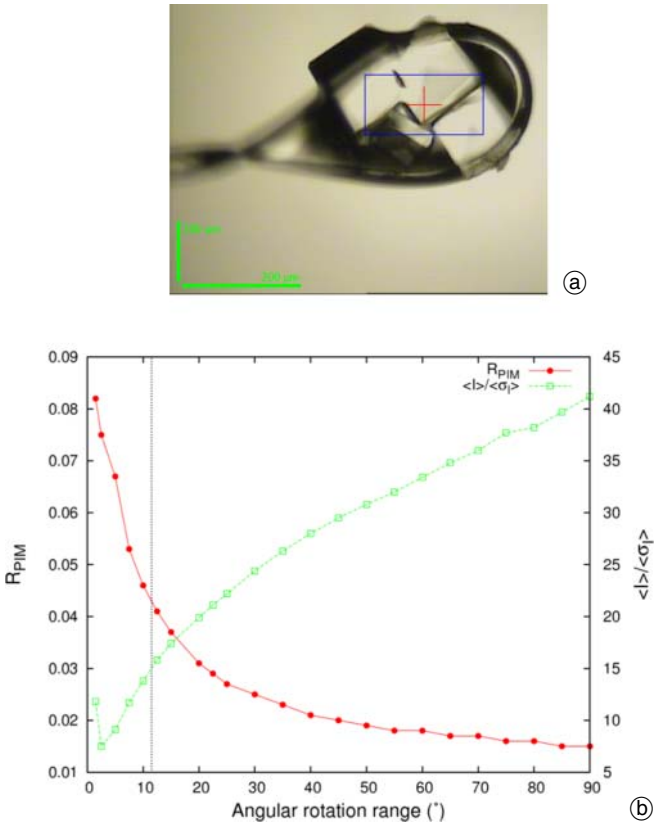

Fig. 4. (**a**) Multiple crystals of insulin in a cryo-loop held at 100 K viewed by an on-axis camera at beamline ID14-4 at ESRF. (**b**) The residual $R_{\text{p.i.m.}}$ and $\langle I\rangle/\langle\sigma_{\text{I}}\rangle$ are plotted as a function of the width of the rotation range included in the data merged from data from four insulin crystals. The vertical dashed line marks the position at which the merged data set is of similar quality to the individual full rotation (90°) data sets from single crystals. (figures are from Paithankar *et al.* (2011)).

remaining crystal, however, had a low mosaicity of 0.2°, and provided a low residual R_{meas} of 0.06 and high $I/\langle\sigma_{\text{I}}\rangle$. Hence, one very good data set was obtained by screening 7 crystals in a single experiment.

This method may become very valuable in the initial stages of the MX structure determination pipeline as an *in situ* crystal screening technique (Jacquamet *et al.*, 2004, 2009; Yadav *et al.*, 2005; Ng *et al.*, 2008). Though the major steps of crystallization, including visualization of drops and identification of possible hits, have been completely automated, X-ray diffraction experiments in MX are slowed by manual selection of crystals to test their diffraction properties. Instead, using the *in situ* method, a plate containing crystallization samples (protein or nucleic acid) in a suitable buffer in hundreds of 'separate drops' could be mounted directly in the X-ray beam by a robot. These plates could be exposed to X-rays in a matter of minutes allowing multiple crystals within a single drop to be irradiated. Coupling of *TotalCryst* programs to these pipelines would accelerate the quick identification of crystallisation conditions giving rise to well diffracting crystals. Alternately, *in situ* data collection at room temperature with chips on microbatch arrays allow for complete datasets that can be used even for an anomalous phasing experiment without significant radiation damage with the help of an ultrafast detector (Kisselman *et al.*, 2011).

7.3 Time-resolved studies in photochemistry

Photocrystallography is the method of choice for studying photoreactions in the solid state since it holds the possibility of studying various aspects of photo-transformation processes. In photocrystallography, an optical light source such as a laser or laser pulse excites the system of interest and the photo-induced structural changes are studied by probing the diffraction signal of the X-ray probe pulses for various time delays (Busse *et al.*, 2003; Davaasambuu *et al.*, 2003; Hallmann *et al.*, 2009; Hallmann and Techert, 2009). There are several strong motivations for introducing the methods of multigrain crystallography in this field:

- An intrinsic problem of the pump-probe experiments is the 2–3 orders of magnitude difference between the penetration depth of the optical pump and the X-ray probe. Measuring properties with standard single crystal diffraction will therefore tend to give rise to problems in interpretation of the results. In order to get an even illumination of the pump throughout the crystal, very small micrometer sized crystals are preferred. These are at best difficult to set up in a single crystal experiment. Multigrain crystallography offers the possibility of extracting single crystal data sets from the polycrystalline samples.
- The powders typically probed are comprised of grains with different sizes, shapes and neighborhoods. Solid-state photochemical reactions are highly dependent on the geometry of the reacting compound and their products. In order to understand the reaction mechanisms, the course of the reactions, and the reaction control factors, it is therefore highly relevant to be able to follow the local structural changes during the reaction. The multigrain crystallography approaches seem ideal for probing the heterogeneity of the time evolution of the structural network either statistically (reaction rates as function of *e.g.* grain sizes) or more ambitiously by acquiring 3D movies of the solid state transformations (see Section 8 below).
- In the rapidly emerging field of stroboscopic laser pump/X-ray probe type experiments used for studies of structural dynamics on the femto- to pico-second scale, the experiments today tend to be severely limited by long data collection procedures. This problem can be substantially reduced by characterizing (artificially made) polycrystals comprising on the order of 10 grains each. Depending on the research topic, these grains may be crystallographically equivalent or represent 10 points in a parameter study. As the compounds studied are typically relatively small molecules, there is ample space in the images for the diffraction spots from 10 grains to be mainly non-overlapping.

Hence, it appears that in addition to the already established methods such as time-resolved Laue diffraction (Makal *et al.*, 2011), monochromatic studies or powder diffraction (Techert *et al.*, 2001), multigrain diffraction methods may have a role to play. The term photo-3DXRD has been coined for such work.

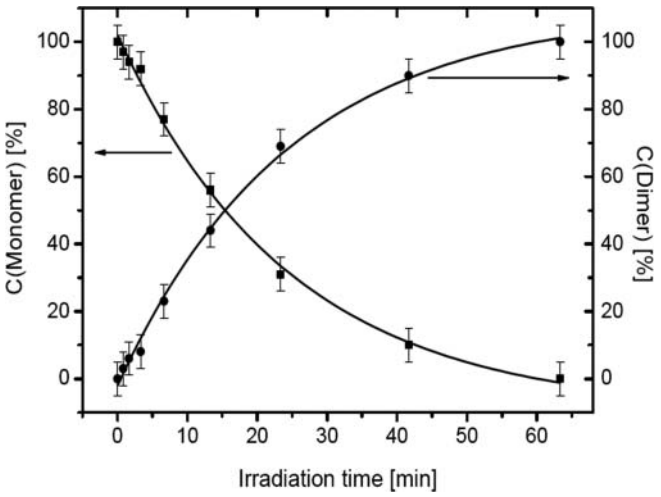

Fig. 5. [2 + 2] cycloaddition reaction of 2-benzyl-5-benzylidene-cyclopentanone. The conversion rate, based on refinements against single-crystal data, from the monomer to the dimer state is shown as changes in molar fraction C as a function of irradiation time.

As an example of this application, we summarise work on the photodimerization of BBCP (Fig. 5) (Davaasambuu *et al.*, 2005). During the reaction, the color of the system as well as its dichroic properties changes, making it an ideal candidate for organic holographic storage devices with evident advantages in the use of polycrystals rather than single crystals.

Since the photocrystallographic studies monitor an irreversible reaction, it is possible to determine the crystal transformation rate directly by refining the occupancy changes from the monomer to the dimer state. The molar fractions of the photo-transformed monomer and dimer have been refined according to a two-phase-model by comparison of the measured Bragg diffraction intensity changes with the structure factors of both pure phases. The molar fraction C(Dimer) of the phototransformed dimer phase has been calculated according to the expression $C(\text{Dimer}) = (I_{\text{tot}}/K - |F(\text{monomer})|^2)(|F(\text{dimer})|^2 - |F(\text{monomer})|^2)$, where K is the product of the multiplicity, the Lorentz factor and the polarization factor. According to this equation, the intensity changes of the Bragg diffraction peaks depend linearly on the number of phototransformed molecules in the crystal. Figure 5 summarises the rate constant as revealed by time-resolved photo crystallography on a single-crystal. For the dimerisation reaction, a transformation time of $\tau_{\text{mono}} = 24\ \text{min} \pm 4\ \text{min}$ for the decrease of the monomer molar fraction and $\tau_{\text{dimer}} = 23 \pm 3\ \text{min}$ for the increase of the dimer molar fraction has been determined. The iso-concentration time point has been found at $\tau_{\text{iso}} = 16.5\ \text{min}$. In the investigated reaction, the ratio of the number of optical photons to the number of chromophores was N(photon): N(chromophore) $\approx 400:1$.

Stochastic analysis. By applying the procedure described above to various grains illuminated during the same experiment and therefore guaranteeing the same optical excitation conditions, a stochastic analysis of the dimerisation rate as a function of grain size and transformation kinetics can be obtained. We performed a stochastic analysis of the phototransformation kinetics of about 10 BBCP microcrystals. Data were measured on beamline ID11 at the ESRF. A 180° rotation range was used with steps of 0.3°. The exposure time was 12 sec/frame. First two measurements were performed at 122 K, followed by a final one at 298 K in order to reach complete dimerisation of the crystals. Hence we got data sets on the pure monomer crystals, on the mixed state and the pure dimer crystals. Further details about the optical excitation conditions (More *et al.*, 2010) as well as the data evaluation procedure (Wright, 2005; Schmidt, 2010; Sørensen, 2008) are described elsewhere. In the structure refinement, performed with the *SHELXL* software (Sheldrick, 2008), the hydrogen atom positions were constrained within a rigid body model. The fraction of spots overlapping was negligible; hence no special care had to be taken in the merging procedure of the reflection data. The monomer and dimer structures were solved and refined for all grains. The average values of R_1 for the pure monomer and dimer structures were 6% and 8%, respectively. Figure 6a summarises the results of these efforts in which the dimerisation rate after 35 minutes of illumination was determined. The size of the crystals studied averages about 10 μm (mean = 10.6 μm). The average dimerisation concentration is at approximately 80% (mean = 78.3%). Crystal grains as small as 6.5 μm in diameter are transformed to about 87% completeness, and grains as big as 15 μm in diameter to about 71%. The crystal thickness was determined from the dimer concentration C(Dimer) by using the rate constants found from the data shown in Fig. 6a. A statistical analysis of another crystal dataset is shown in Figs. 6b and c. For this grain set a mean size of 76.3 ± 1.7 μm and a median of 77 μm was obtained (Fig. 6b). The distribution of the dimer formation as a function of grain sizes is shown in Fig. 6c. The observed distribution is Poissonian, although there are only 11 data points. Nonetheless, Fig. 6c demonstrates the power of photo-3DXRD for characterisation of polycrystalline materials with photo-reactivity.

7.4 Discussion

Prior to starting our research on multigrain crystallography, it was anticipated that spot overlap would be its main limitation. The work presented above demonstrates that the algorithmic approaches developed can handle substantial fractions of overlap. Furthermore, we find that the overlap of spots associated with different grains tend to be random in nature. This is in contrast to the familiar situation with Laue single crystal diffraction, where spot overlap is known to cause systematic absences in the set of integrated intensities, which in turn has proved to be a barrier to the Laue technique becoming generally applicable for MX.

During the project we have realized that another limitation is related to the heterogeneous nature of the samples themselves. As already mentioned, the grains may vary by orders of magnitude in size and mosaic spread. In some cases the result will be a strongly varying "powder diffraction" background, which in order to follow the procedures presented above must be separated from the spots from the larger grains. This calls for improved algorithms, pos-

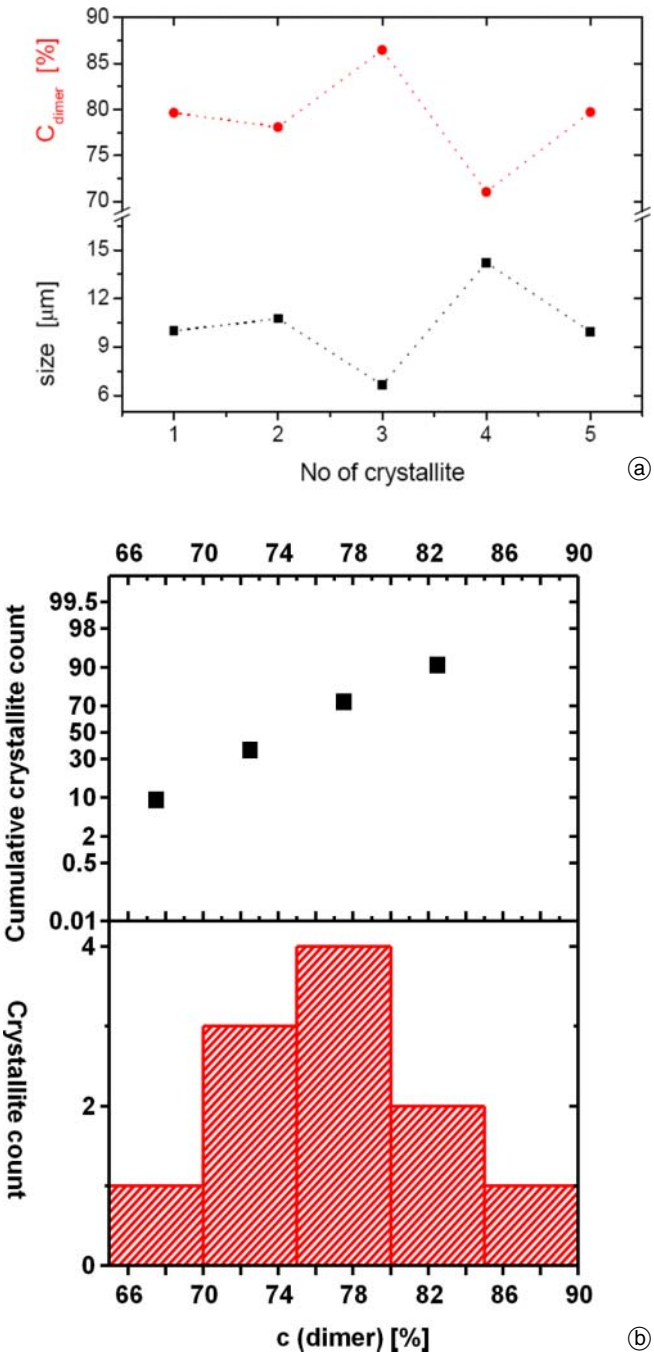

Fig. 6. (**a**) Correlation of the dimer concentration and size of the transformed crystallites as determined by photo-3DXRD. (**b**)–(**c**) Statistical analysis of the conversion rates during the photoreaction for various crystallites. (**c**) Photo-transformation rates of single particle micro-grains of various sizes under the same illumination conditions.

sibly involving several iterations between integration and refinement steps.

A different solution would be to consider the sample not as comprised of an assemblage of grains but rather as *one single crystal with an unusual, very broad and spiky type of orientation distribution.* By analogy to Section 5.1 such a "textured single crystal" will be associated with an ODF, which is the sum of all the single grain ODFs. This ODF is to be generated based on the entire intensity distribution within 5–10 selected, isolated Debye-Scherrer rings. Once the ODF is known, each {*hkl*}-family can be associated with an intensity distribution (peak-shape function). Integrated intensities are then found by fitting to this unusual type of peak-shape function. Structure determination proceeds by standard single crystal methods. It appears that this formalism holds the prospect of single crystal quality refinements even in the limit of severe spot overlap, where the approach in Section 5.1 may fail. The disadvantage is that no grain statistics are provided. The two approaches may be combined, *e.g.* a selected grain may be characterized by the multigrain formalism, while the intensity from all other grains is treated as a "background" to be characterized by the textured single crystal formalism. Work on this approach is ongoing.

Next we comment on the use of the concept of multigrain crystallography more generally. We note that this applies naturally to laboratory X-ray sources, as the only requirements are the use of a monochromatic beam, a rotation stage and a 2D detector. Furthermore, we foresee that it may be relevant in connection with the new generation of neutron sources (SNS, J-PARC and ESS), where sample volumes can be relatively small.

It is also envisioned that the multigrain approach will be of use for structural and crystallographic studies of polycrystalline materials at 4th generation X-ray sources; that is the hard X-ray free electron lasers (FELs). First experiments with FEL radiation (Rajkovic *et al.*, 2010; Rajkovic *et al.*, 2010; Hallmann *et al.*, 2010) indicate such a possibility. Explicitly in this context, we can compare Laue diffraction images made by broadband Laue radiation as generated with a wiggler at a 2nd generation synchrotron (5–20 keV radiation, F1 beamline, DORIS, DESY, Hamburg) (Fig. 7b), pink X-ray radiation generated by an undulator at a 3rd generation synchrotron (16.5 keV, ID09B beamline, ESRF, Grenoble) (Fig. 7c) and pink X-ray radiation from a 4th generation X-ray source (16 keV, XPP beamline, LCLS, SLAC, Stanford) (Fig. 7d). The sample investigated was in all cases single crystals of Rh_2(1,8-diisocyano-*p*-menthane)$_4 * PF_4$, abbreviated as Rh_2(dimen)$_4$. Figure 7 shows that the observation of Laue diffraction to high spatial resolution is possible with all kinds of currently available hard X-ray sources ranging from 2nd generation sources to 4th generation sources. Due to the high degree of monochromaticity of the FEL radiation ($\Delta E/E = 10^{-3}$) the multigrain approach described in this paper can be combined with the crystallographic pink-Laue collection strategies which would allow the intensities of diffraction peaks to be disentangled.

8. TotalCrystallography

Historically, the concept of multigrain crystallography (Schmidt *et al.*, 2003; Vaughan *et al.*, 2004) has been developed in parallel with 3DXRD microscopy (Poulsen, 2004; Juul Jensen *et al.*, 2006). With 3DXRD and derivatives such as Diffraction Contrast Tomography (DCT) (Ludwig *et al.*, 2008) the aim is to generate 3D maps of up to a thousand grains within metals and ceramics and to characterize the individual properties of these grains, such as their crystalline orientation or stress state. Furthermore, the goal is to generate such maps sufficiently rapidly that it becomes

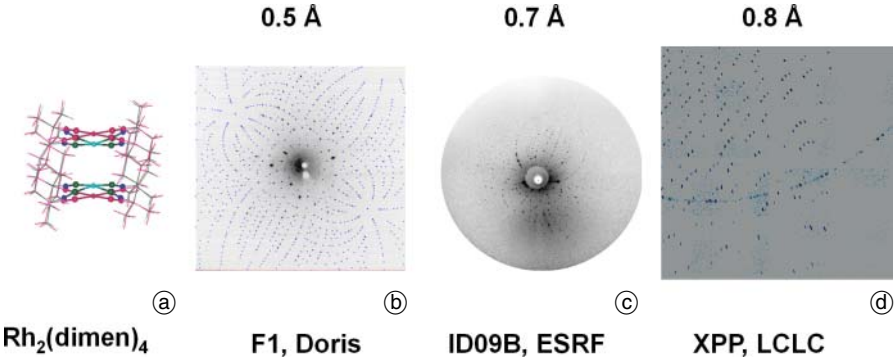

Fig. 7. Laue diffraction of Rh_2(1,8-diisocyano-p-menthane)$_4 * PF_4$ [(Rh_2(dimen)$_4$] single crystals investigated at various X-ray sources of large scale facilities. (**a**) structure of Rh_2(dimen)$_4$. (**b**) Laue pattern of Rh_2(dimen)$_4$ from a 2nd generation synchrotron, (**c**) pink-Laue pattern from a 3rd generation synchrotron and (**d**) pink-Laue pattern from a 4th generation X-ray source[4].

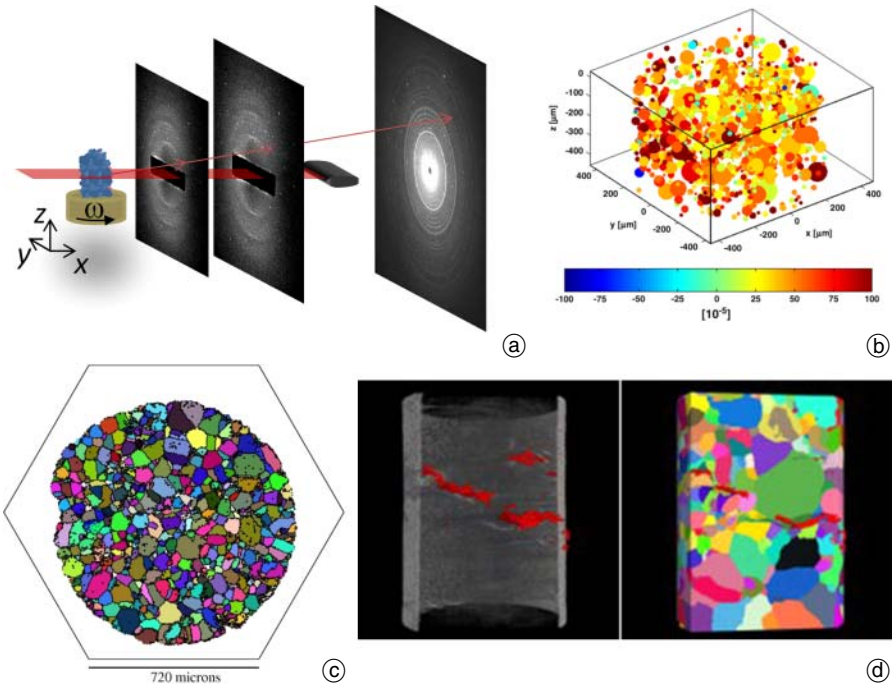

Fig. 8. 3DXRD overview. (**a**) Experimental set-up. (**b**)–(**d**) examples of resulting 3D maps. (**b**) Map revealing the position, volume (given by size of sphere) and axial strain of 1118 grains within a polycrystalline Cu sample with the strain level indicated by the bar (Oddershede *et al.*, 2011). (**c**) one section of a 3D grain map of a cylindrical shaped Ni sample with colors representing the orientations of the grains (Hefferan *et al.*, 2009). (**d**) Combined density map from tomography with cracks highlighted in red and a grain orientation map, revealing how the cracks propagate with respect to grain boundaries. From a study on stainless steel by King *et al.* (2008).

possible to make movies of the grain dynamics during processing steps such as annealing or plastic deformation.

The setup currently used for 3DXRD at beamline ID11 at the ESRF is shown in Fig. 8, and details of the current state of hardware and software/algorithms used for this work can be found in Vaughan *et al.* (2010) and Poulsen *et al.* (2010), respectively. Notably, several detectors are used: two semitransparent nearfield high spatial resolution detectors and a classical high count rate crystallography area detector at a much larger distance. The former detectors provide the relevant spatial information while the latter has a superior angular resolution. To illustrate the status of 3DXRD, a few selected maps are shown in Fig 8. Note in particular example D), where a grain map is superposed on a simultaneously acquired 3D density map based on X-ray tomography: this combination is very useful for studies of porous materials or for studies of crack propagation (King *et al.*, 2008). Typically the spatial resolution of 3DXRD is 1–3 μm. A recent publication demonstrates the use of 3DXRD in geoscience in a study of the development of strain in sand grains under macroscopic compression (Hall *et al.*, 2011).

The 3DXRD results presented above all relate to monophase materials of a known structure. For studies of typical materials such as polycrystalline aluminum, crystal structure determination is not an objective.

TotalCrystallography is defined as the simultaneous characterization of the 3D atomic, and the 3D grain-scale structure of polycrystalline samples with unknown phase(s) as well as the temporal characteristics of such samples. In other words the objective is to combine the atomic-scale analysis of single crystal diffraction with the grain scale methodology of materials science, providing a universal multi-scale framework.

In practice we intend to pursue *TotalCrystallography* with the same set-up as used for 3DXRD, shown in Fig. 8a. Furthermore, we will first implement solutions that in some aspects are a hybrid between existing 3DXRD, tomography (optional, see below) and multigrain crystallo-

[4] The hard X-ray FEL experiments were performed at the XPP beamline of LCLS. M. Messerschmidt, D. Fritz, M. Cammaratta, H. Lemke, S. Boutet, G. Williams, M. Scholz and S. Techert contributed to the experiment.

graphy algorithms. This generalization requires the grain dimensions to be larger than the resolution of the near-field detectors for 3DXRD, which is currently a few μm.

The advantage of *TotalCrystallography* for conventional crystallographic studies in *e.g.* the pharmaceutical industry would be that the spatial information provided may increase the fidelity of the polycrystal indexing methods substantially, as well as reducing the number of mis-indexed peaks and thereby improving the quality of the refinements. This has been seen to be the case in several test samples. Moreover 3D maps may sometimes be of interest in themselves, *e.g.* for probing the heterogeneity of drug tablets, or for identifying the 3D position of the high quality grain.

Perhaps more importantly, we see a clear need for *TotalCrystallography* in geosciences, and in materials science. In both disciplines, heterogeneous multiphase samples with sometimes unknown phases are commonplace, and there is a strong desire to develop and/or validate structural models that bridge length scales (by probing the sample on the atomic and mesoscopic length scale simultaneously). Most of the polycrystalline indexing and mapping programs presented above such as *GrainSpotter* (Schmidt, 2010) and *GrainSweeper* (Schmidt, 2005) are currently only implemented for mono-phase materials. Hence, in order to use the existing software, intermediate steps are required that divide the diffraction data into sets, with each set representing one phase. We present two strategies:

- *Division based on angular information*. It is assumed that the sample is known to comprise only a few phases, which furthermore belong to a finite list of known structures. In the simplest case, scattering angles 2θ uniquely define to which phase a given reflection belongs and the division is trivial. In the case of a minor degree of overlap in 2θ between phases, an indexing program such as *GrainSpotter* can be run independently for each of the candidate phases, setting tight limits on the 2θ ranges included in the analysis. Erroneous combinations of reflections will be filtered out by the completeness of other criteria.
- *Division based on real space data.* This is a potential solution for both known and unknown phases. Near-field 3DXRD data can be used if the grains are sufficiently larger than the spatial resolution of the technique. In this case, ray tracing of diffraction spots is used to extrapolate the centre-of-mass of the grain of origin. If the grain centre-of-masses cluster sufficiently in 3D space, this suggests a way to divide the far-field data. The real space division may be complemented by absorption or phase contrast tomography, either carried out simultaneously or subsequently to the acquisition of diffraction data. If the electron densities of the phases are sufficiently different one can segment the resulting 3D tomogram to obtain 3D maps of each of the phases with a high spatial resolution. This can then be used to help sort the diffraction data based on a comparison of the extrapolated positions from the near-field data and the tomogram. Note in this connection that the spatial resolution of 3DXRD is a few microns, while state-of-the-art tomography set-ups at synchrotrons have sub-micron resolution for mm-sized specimens and 50 nm resolution for nano-crystalline specimens (Mokso *et al.*, 2007). Another advantage is that tomography also works for cases where parts of the sample will not provide useful multigrain diffraction patterns, *e.g.* due to nano-crystallinity, or texture. The main disadvantage of including tomography is the increased complexity in instrumentation and data analysis, but as tomographic detectors can be fairly straightforwardly inserted into our current compound detector schemes, and tomographic data analysis is very mature, these limitations are not seen as prohibitive.

For example, in a combined 3DXRD and tomography study of chalk, the division was based on angular information. Chalk, a natural porous multiphase material, is a very important material in nature acting both as aquifers and oil reservoirs worldwide. It primarily consists of calcite, $CaCO_3$, but can contain a number of different other minerals, *e.g.* clays and quartz. In this study (Sørensen *et al.*, 2011), the microstructure and topology of the porous network was determined by X-ray microtomography at the Swiss Light Source with a voxel resolution of 0.35 μm. A slice in the reconstructed tomogram is shown in Fig. 9. From the intensity variations which are related to the linear absorption coefficients, it is obvious that many high density inclusions are buried in the bulk of the nano-crystalline chalk. To obtain a complete description of the sample, we sought to identify the mineral type of these inclusions by performing a 3DXRD experiment on the same

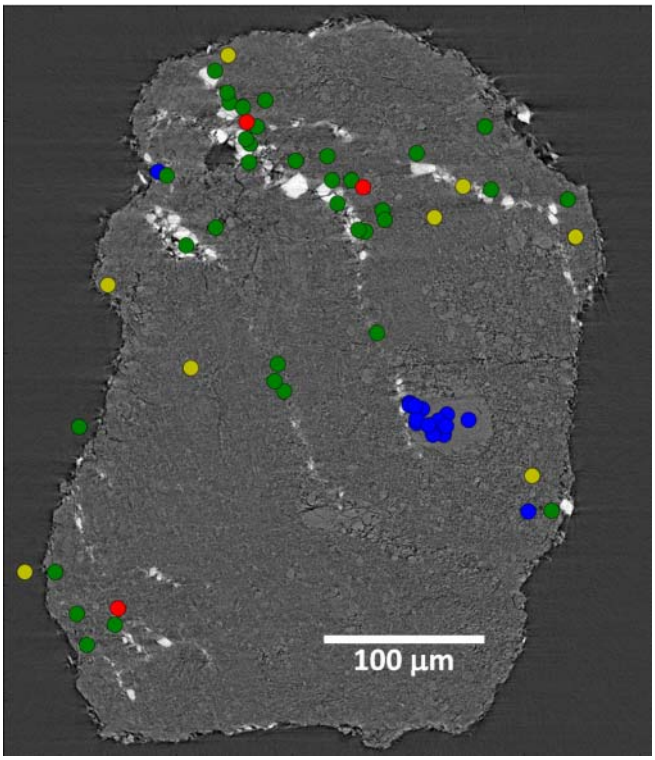

Fig. 9. Slice of a 3D map of chalk. The spatial positions of grains from four different minerals were determined by *GrainSpotter* (Schmidt, 2010). Calcite grains are blue, quartz, yellow, barite, green, and pyrite, red. Their postions are superimposed on a density map of the same sample, generated by X-ray tomography (figure is from Sørensen *et al.*, 2011).

sample at beamline ID11 at ESRF. For the latter study high energy X-rays (55 keV) were used and a segment of the sample was mapped layer by layer with a 1200 μm × 5 μm beam. Diffraction images were collected while rotating the sample over 200° in steps of 0.5° and with an exposure time of 6 sec. In this case the resolution of the centre-of-mass positions of the crystals was 10 μm.

By use of Mössbauer spectroscopy and powder diffraction on ground chalk, as well as geological relationships, a catalogue of 11 possible phases was made to guide for which minority phases to search in the 3DXRD data. Based on trial and error, from this list, successful indexing of four mineral types was achieved with *GrainSpotter*. The inclusions, which were easily observed in the tomogram, were found to be mainly barite (35 crystal orientations were matched), but also a small quantity of pyrite (3 crystals). The positions of these crystals are shown as green and red circles in Fig. 9. Minor off-sets are observed in the positions of the crystals in the tomogram and the 3DXRD map, because of alignment issues related to measurements being performed at different experimental stations. Despite this uncertainty, a good correlation was found between the spatial position of the grains found in the 3DXRD experiment and the position of the inclusions in the tomogram.

Apart from the denser minerals, barite and pyrite, a few grains of quartz were also observed. However, it is difficult to observe these grains in the tomogram because they are small and the linear absorption coefficients for calcite and quartz are very similar. Generally the calcite crystals that arise from coccoliths, the predominant source of calcite in chalk, are less than 100 nm in size, and appear as powder rings in the diffraction images, but some calcite crystals could be indexed, indicating different genesis. These larger calcite grains are shown as blue circles in Fig. 9.

The above discussion has focused on the extension of existing software originally developed for either multigrain crystallography (using farfield data only) or 3DXRD (nearfield mapping of known phases) towards *TotalCrystallography*. We emphasise the need for a new generation of programs, tailored specifically to this challenging goal. Such work is currently in progress, and will be reported elsewhere.

9. Conclusions

Multigrain crystallography applications within a range of disciplines have been demonstrated. The quality of the resulting refinements is comparable to single crystal work. The simulations indicate that the method is applicable for samples of simple metals, typical small organic molecules and proteins with up to a thousand grains, a few hundred grains and about ten grains, respectively. These findings sustain our argument that multigrain crystallography should be seen as a general tool for crystallographic studies: a third method that is complementary to the traditional single crystal and powder diffraction approaches.

The work on generalizing multigrain crystallography to *TotalCrystallography* is still in its infancy as X-ray crystallography was in 1912 with Friedrich, Knipping and Laue's first paper on the subject. First results have been obtained by combining 3DXRD, tomography and multigrain crystallography methods in a similarly *ad hoc* manner as the experiment in 1912.

Acknowledgments. We acknowledge stimulating scientific discussions with A. Frost Jensen, G. T. Herman, I. Kazantsev, S. Larsen, F. Krebs Larsen, A. G. W. Leslie, H. Powell, R. M. Suter, Z. Sükösd, P. C. Hansen and S. Stipp. L. Margulies participated in the experimental work. Samples were kindly provided by A. Frost Jensen and H. Lopez de Diego, H. Lundbeck A/S and F. Engstrøm, Maersk Oil. The FABLE modules were in part programmed by G. Suchet, A. Götz, K. Evans and E. Knudsen. M. Dusek and V. Petricek made the necessary generalizations of JANA. We thank W. Schmahl for useful suggestions for improving this paper. We thank ESRF and HASYLAB for beamtime. Financial support was granted by the EU 6th Framework NEST/ADVENTURE project TotalCryst, by the Danish National Research Foundation and by the Danish Councils for Independent Research via the center Danscatt.

References

Ch. Baerlocher, L. B. McCusker, S. Prokic, T. Wessels, *Z. Kristallogr.* **2004**, *219*, 803–812.
G. I. Berglund, G. H. Carlsson, A. T. Smith, H. Szöke, A. Henriksen, J. Hajdu, *Nature* **2002**, *417*, 463–468.
J. Bernstein, *Polymorphism in Molecular Crystals*, Oxford University Press, New York **2002**.
W. L. Bragg, The Specular Reflection of X-rays. *Nature*, **1912**, *90*, 410.
W. R. Busing, H. A. Levy, *Acta Cryst.* **1967**, *22*, 457–464.
G. Busse, Th. Tschentscher, A. Plech, M. Wulff, B. Frederichs, S. Techert, *Faraday Discuss*. **2003**, *122*, 105–117.
L. Buts, M.-H. Dao-Thi, L. Wyns, R. Loris, *Acta Cryst. D* **2004**, *60*, 983–984.
J. W. Campbell, *J. Appl. Cryst.* **1998**, *31*, 407–413.
J. Davaasambuu, G. Busse, S. Techert, *J. Phys. Chem. A* **2010**, *110*, 3261–3265.
J. Davaasambuu, G. Busse, S. Techert (2005) *J. Phys. D: Appl. Phys.*, **38**, A204–A207.
W. I. F. David, L. B. McCusker, Ch. Baerlocher, *Structure Determination from Powder Diffraction Data*, Oxford University Press, Oxford **2002**.
P. Debye and P. Scherrer, Interferenzen an regellos orientierten Teilchen im Röntgenlicht. I. Nachrichten der kgl. Gesellsch. d. Wiss. Göttingen, **1916**, *1*, 1–15
A. J. M. Duisenberg, *J. Appl. Cryst.* **1992**, *25*, 92–96.
A. J. M. Duisenberg, *Reflections on Area Detectors*, Ph.D. thesis, (Utrecht) **1998**.
M. Dusek, V. Petricek, M. Wunschel, R. E. Dinnebier, S. van Smaalen, *J. Appl. Cryst*. **2001**, *34*, 398–404.
F. C. Frank, *Metall. Mater. Trans A* **1988**, *19*, 403–408.
W. Friedrich, P. Knipping, M. Laue, Interferenz-Erscheinungen bei Röntgenstrahlen. *Sitzungsberichte der Königlich Bayerischen Akademie der Wissenschaften, Mathematisch – physikalische Klasse*, **1912**, 303–322.
W. Friedrich, P. Knipping, M. Laue, *Ann. D. Phys.* **1913**, *41*, 971–988.
H. Graafsma, S. O. Svensson, Å. Kvick, *J. Appl. Cryst.* **1997**, *30*, 957–962.
S. A. Hall, J. Wright, T. Pirling, E. Ando, D. J. Hughes, G. Viggiani, *Granular Matter* **2011**, *13*, 251–254.
J. Hallmann, W. Morgenroth, C. Paulmann, J. Davaasambuu, Q.-Y. Kong, M. Wulff, S. Techert, *J. Am. Chem. Soc.* **2009**, *131*, 15018–15025.
J. Hallmann, S. Techert, *J. Phys. Chem. Lett.* **2010**, *1*, 959–961.
J. Hallmann, W. Quevedo, G. Grübel, I. Rajkovic, G. Busse, R. Moré, M. Petri, S. Techert, *J. Phys. B: At. Mol. Opt. Phys.* **2010**, *43*, 194009–194016.
P. C. Hansen, H. O. Sørensen, Z. Sükösd, H. F. Poulsen, *SIAM J Imaging Sciences* **2009**, *2*, 593–613.

K. D. M. Harris, M. Tremayne, B. M. Kariuki, *Angew. Chem. Int. Ed.* **2001**, *40*, 1626–1651.
C. M. Hefferan, S. F. Li, J. Lind, U. Lienert, A. D. Rollett, P. Wynblatt, R. M. Suter, *Computers, Materials and Continua* **2009**, *14*, 209–219.
G. T. Herman. *Image Reconstruction from Projections*, Academic Press, New York **1980**.
L. Jacquamet, J. Ohana, J. Joly, F. Borel, M. Pirocchi, P. Charrault, A. Bertoni, P. Israel-Gouy, P. Carpentier, F. Kozielski, D. Blot, J.–L. Ferrer, *Structure* **2004**, *12*, 1219–1225.
L. Jacquamet, J. Joly, A. Bertoni, P. Charrault, M. Pirocchi, X. Vernede, F. Bouis, F. Borel, J.–P. Périn, T. Denis, J.-L Rechatin, J.-L Ferrer, *J. Synchrotron Rad.* **2009**, *16*, 14–21.
D. Juul Jensen, E. M. Lauridsen, L. Margulies, H. F. Poulsen, S. Schmidt, H. O. Sørensen, G. B. M. Vaughan, *Mater. Today* **2006**, *9*, 18–25.
W. Kabsch, *J. Appl. Cryst.* **1988**, *21*, 916–924.
P. Kenesei, *DIGIgrain manual*, Eötvös Loránd University, Budapest **2010**.
A. King, G. Johnson, D. Engelberg, W. Ludwig, J. Marrow, *Science* **2008**, *312*, 382–385.
G. Kisselman, W. Qiu, V. Romanov, C. M. Thompson, R. Lam, K. P. Battaile, E. F. Pai, N. Y. Chirgadze, *Acta Cryst D* **2011**, *67*, 533–539.
U. F. Kochs, C. N. Tome, H. R. Wenk. *Texture, Anisotropy*, Cambridge University Press, Cambridge **1998**.
E. M. Lauridsen, S. Schmidt, R. M. Suter, H. F. Poulsen, *J. Appl. Cryst.* **2001**, *34*, 744–750.
A. G. W. Leslie. *Acta Cryst. D* **2006**, *62*, 48–57.
W. Ludwig, P. Reischig, A. King, M. Herbig, E. M. Lauridsen, G. Johnson, T. Marrow, J.-Y. Buffiere. *Rev. Sci. Instrum.* **2009**, *80*, 33905-0–33905-9.
W. Ludwig, S. Schmidt, E. M. Lauridsen, H. F. Poulsen, *J. Appl. Cryst.* **2008**, *41*, 302–309.
A. Lyckegaard, A. Alpers, W. Ludwig, R. W. Fonda, L. Margulies, A. Götz, H. O. Sørensen, S. R. Dey, H. F. Poulsen, E. M. Lauridsen, 3D grain reconstruction from boxscan data. In: *Proceedings of the 31st Risø International Symposium on Materials Science* (Eds N. Hansen, D. Juul Jensen, S. F. Nielsen, H. F. Poulsen, B. Ralph), p. 329–336. Risø National Laboratory for Sustainable Energy, Technical University of Denmark, (Roskilde, Denmark) 2010.
A. Makal, E. Trzop, J. Sokolow, J. Kalinowski, J. Benedict, P. Coppens, *Acta Cryst. A* **2011**, *67*, 319–326.
M. Messerschmidt, G. Busse, J. Davaasambuu, M. Camaratta, A. Meens, T. Tschentscher, S. Techert, *J. Phys. Chem. A* **2010**, *114*, 7677–7681.
L. Meister, H. Schaeben, *Math. Meth. Appl. Sciences* **2005**, *28*, 101–126.
R. Mokso, P. Cloetens, E. Maire, W. Ludwig, J.-Y. Buffière, *Appl. Phys. Lett.* **2007**, *90*, 144104-1–144104-3.
R. More, G. Busse, J. Hallmann, C. Paulmann, M. Scholz, S. Techert, *J. Phys. Chem. C* **2010**, *14*, 4142–4148.
M. Moscicki, P. Kenesei, J. Wright, H. Pinto, T. Lippmann, A. Borbély, A. R. Pyzalla, *Materials Science and Engineering: A* **2009**, *524*, 64–68.
J. Oddershede, S. Schmidt, H. F. Poulsen, L. Margulies, J. Wright, M. Moscickic, W. Reimers, G. Winther, *Materials Characterization* **2011**, *62*, 651–660.
J. Oddershede, S. Schmidt, H. F. Poulsen, H. O. Sørensen, J. Wright, W. Reimers, *J. Appl. Cryst.* **2010**, *43*, 539–549.
J. Oddershede, B. Camin, S. Schmidt, L. P. Mikkelsen, H. O. Sørensen, U. Lienert, H. F. Poulsen. W. Reimers, *in preparation* **2011**.
Z. Otwinowski, W. Minor, Processing of X-ray diffraction data collected in oscillation mode. In: *Macromolecular Crystallography, Part A* (Eds C. W. J. Carter, R. M. Sweet), Methods in Enzymology, Vol. 276, p. 307–326. Academic Press, (New York) 1997.
K. S. Paithankar, H. O. Sørensen, J. P. Wright, S. Schmidt, H. F. Poulsen, E. F. Garman, *Acta Cryst. D* **2011**, *67*, 608–618.
V. Petricek, M. Dusek, *Z. Kristallogr.* **2004**, *219*, 692–700.
H. F. Poulsen, *Three-Dimensional X-ray Diffraction Microscopy*, Springer, Berlin **2004**.
H. F. Poulsen, S. F. Nielsen, E. M. Lauridsen, S. Schmidt, R. M. Suter, U. Lienert, L. Margulies, T. Lorentzen, D. Juul Jensen, *J. Appl. Cryst.* **2001**, *34*, 751–756.
H. F. Poulsen, W. Ludwig, E. M. Laudriensen, S. Schmidt, W. Pantleon, U. L. Olsen, J. Oddershede, P. Reischig, A. Lyckegaard, J. P. Wright, G. B. M. Vaughan, 4D characterization of metals by 3DXRD techniques. In: *Proceedings of the 31st Risø International Symposium on Materials Science* (Eds. N. Hansen, D. Juul Jensen, S. F. Nielsen, H. F. Poulsen, B. Ralph), p. 101–119. Risø National Laboratory for Sustainable Energy, Technical University of Denmark, (Roskilde, Denmark) 2010.
S. O. Poulsen, E. M. Lauridsen, A. Lyckegaard, J. Oddershede, C. Gundlach, C. Curfs, D. Juul Jensen, *Scripta Mater.* **2011**, *64*, 1003–1006.
H. R. Powell, *Acta Cryst. D* **1999**, *55*, 1690–1695.
I. Rajkovic, G. Busse, J. Hallmann, R. More, M. Petri, W. Quevedo, F. Krasniqi, A. Rudenko, T. Tschentscher, N. Stojanovic, S. Düsterer, R. Treusch, M. Tolkiehn, S. Techert, *Phys. Rev. Lett.* **2010**, *104*, 125503-6.
I. Rajkovic, J. Hallmann, S. Grübel, R. More, W. Quevedo, M. Petri, S. Techert, *Rev. Sci. Instr.* **2010**, *81*, 045105-1-6.
R. B. G. Ravelli, E. F. Garman, *Curr. Opin. Struct. Biol.* **2006**, 16, 624–629.
S. Schmidt, *GrainSpotter v. 0.82*, http://fable.svn.sourceforge.net/svnroot/fable/GrainSpotter., Risø National Laboratory for Sustainable Energy, Technical University of Denmark, (Roskilde) 2010.
S. Schmidt, *GrainSweeper*, http://fable.svn.sourceforge.net/svnroot/fable/GrainSweeper. Risø National Laboratory for Sustainable Energy, Technical University of Denmark, (Roskilde) 2005.
S. Schmidt, H. F. Poulsen, G. B. M. Vaughan, *J. Appl. Cryst.* **2003**, *36*, 326–332.
A. M. M. Schreurs, X. Xian, L. M. J. Kroon-Batenburg, *J. Appl. Cryst*. **2010**, *43*, 70–82.
G. M. Sheldrick, *Acta Cryst. A* **2008**, *64*, 112–122.
G. M. Sheldrick, *Acta Cryst. A* **1990**, *46*, 467–473.
R. Sparks, *GEMINI*, Bruker-AXS, Inc. Madison, WI **1999**.
T. Straasø, D. Müeter, H. O. Sørensen, J. Als-Nielsen, *In preparation* **2011**.
H. O. Sørensen, *fabric*, http://fable.svn.sourceforge.net/svnroot/fable/fabric. Risø National Laboratory for Sustainable Energy, Technical University of Denmark, (Roskilde) 2007.
H. O. Sørensen, *PolyXSim – 3DXRD Far-field Simulation of Polycrystals*, http://fable.svn.sourceforge.net/svnroot/fable/simulation/PolyXSim. Risø National Laboratory for Sustainable Energy, Technical University of Denmark, (Roskilde) 2008.
H. O. Sørensen, S. Hakim, S. Pedersen, S. Schmidt, C. P. Hem, I. S. Pasarin, C. Frandsen, Z. I. Balogh, U. L. Olsen, J. Oddershede, B. C. Christiansen, R. Feidenhans'l, S. L. S. Stipp, **2011**, *To be submitted*.
H. O. Sørensen, S. Larsen, *Acta Cryst. B* **2003**, *59*, 132–140.
H. O. Sørensen, S. Larsen, *J. Appl. Cryst.* **2003**, *36*, 931–939.
S. Techert, F. Schotte, M. Wulff, *Phys. Rev. Lett.* **2001**, *86*, 2030–2034.
G. B. M. Vaughan, S. Schmidt, H. F. Poulsen. *Z. Kristallogr.* **2004**, *219*, 813–825.
G. B. M. Vaughan, J. P. Wright, A. Bychkov, C. Curfs, C. Gundlach, M. Orlova, L. Erra, H. Gleyzolle, T. Buslaps, A. Gotz, G. Suchet, S. Petitdemange, M. Rossat, L. Margulies, W. Ludwig, A. Snigirev, I. Snigireva, S. Schmidt, H. O. Sørensen, E. M. Lauridsen, U. L. Olsen, J. Oddershede, H. F. Poulsen, The extension of ID11 for nanoscale and hierarchical characterization. In: *Proceedings of the 31st Risø International Symposium on Materials Science* (Eds N. Hansen, D. Juul Jensen, S. F. Nielsen, H. F. Poulsen, B. Ralph), p. 457–476. Risø National Laboratory for Sustainable Energy, Technical University of Denmark, (Roskilde, Denmark) 2010.
G. B. M. Vaughan, *Merge*, http://fable.svn.sourceforge.net/svnroot/fable/Merge. ESRF, (Grenoble) 2008.
G. B. M. Vaughan, et al., in preparation 2011.
T. Wessels, Ch. Baerlocher, L. B. McCusker, *Science* **1999**, *284*, 477–479.
S. West, S. Schmidt, H. O. Sørensen, G. Winther, H. F. Poulsen, L. Margulies, C. Gundlach, D. Juul Jensen, *Scripta Mater.* **2009**, *61*, 875–878.
J. Wright, *ImageD11*, http://fable.svn.sourceforge.net/svnroot/fable/ImageD11/. ESRF, (Grenoble) 2005.
M. K. Yadav, C. J Gerdts, R. Sanishvili, W. W Smith, L . S. Roach, R. F. Ismagilov, P. Kuhn, R. C. Stevens, *J. Appl. Cryst.* **2005**, *38*, 900–905.